

Tropical thermocline helps power Pacific equatorial upwelling

Noel G. Brizuela^{a,*}, Chia-Ying Lee^a, Adam H. Sobel^{a,b}, Richard Seager^a, Suzana J. Camargo^a,
Jing-Yi Zhuo^a

^a *Lamont-Doherty Earth Observatory, Columbia University, New York, NY, USA*

^b *Department of Applied Physics and Applied Mathematics, Columbia University, New York, NY,
USA*

This is a non-peer-reviewed preprint. The manuscript has been submitted to the J

Corresponding author: Noel G. Brizuela, noel.brizuela@mpimet.mpg.de

**Current affiliation:* Max Planck Institute for Meteorology, Hamburg, Germany

9 ABSTRACT: Upwelling in the equatorial Pacific Ocean exerts a primary influence on the Earth's
10 climate, but there is great uncertainty on whether this influence will intensify or weaken under
11 global warming. The dominant dynamical theory of equatorial upwelling argues that the easterly
12 trade winds 'pull' water up towards the surface via Ekman suction. In contrast, studies of decadal
13 variability suggest that the subtropical cells 'push' equatorial upwelling from below. Therefore, it
14 is unclear whether upwelling is 'pulled from above' by Ekman divergence or 'pushed from below'
15 by geostrophic convergence. Here, we use a framework of local available energetics to study
16 the Pacific shallow overturning circulation and find that at least 20-50% of equatorial upwelling
17 cannot be powered directly by winds along the equator, as commonly understood. Instead, this
18 fraction of upwelling is powered by potential energy that is transferred to the thermocline via
19 off-equatorial downwelling and diabatic processes. Water parcels holding excess potential energy
20 in the equatorial thermocline are then able to upwell without additional energy input, such that
21 equatorial upwelling can in fact be pushed from below. The strength of this push is largely set
22 by the trade winds, but may also be influenced by energy sources across the subtropical ocean.
23 Unlike previous available energetics analyses of the equatorial region, our study uses complete
24 local conservation laws that allow us to trace all energy sources and pathways. This makes our
25 dynamical formulation particularly useful to explain variations in equatorial Pacific upwelling at
26 interannual and decadal timescales alike.

27 **1. Introduction**

28 Upwelling in the equatorial Pacific Ocean sets the zonal sea surface temperature (SST) gradient
29 that regulates the tropical atmospheric circulation. Therefore, variations in equatorial upwelling
30 can induce shifts in global climate. At interannual timescales, these shifts are typically associated
31 with fluctuations in the trade winds and the Equatorial Current System (ECS) via the Bjerknes
32 feedback (Zebiak and Cane 1987). In turn, decadal variability is linked to subsurface equatorward
33 flows that close the Subtropical Cells (STCs) (Luo et al. 2003; Capotondi et al. 2023). Because
34 the ECS and STCs are inextricably connected by equatorial upwelling (Lu et al. 1998), dynamical
35 understanding of future changes in Pacific Ocean climate requires that ECS- and STC-based views
36 of variability be compatible.

37 Interactions between the STCs and the ECS are well documented, but untangling the dynamical
38 and thermodynamical aspects of these interactions remains a challenge. One obstacle is that the
39 ECS and STCs are thought to regulate equatorial upwelling velocities by different and seemingly
40 unrelated mechanisms. The ECS view of equatorial upwelling has the thermocline ‘pulled from
41 above’, as easterly winds drive meridional divergence in the Ekman layer (Wyrski 1981). In
42 contrast, Kleeman et al. (1999) suggested that speeding up of the STCs can enhance meridional
43 convergence of thermocline flows around the equator and thus strengthen upwelling by ‘pushing
44 from below’.

45 Interactions between the ECS and STCs have received increased attention in recent years, as
46 observations indicate net cooling of the cold tongue SST over past decades (Karnauskas et al.
47 2009). Virtually all climate models fail to accurately reproduce historical cooling in the cold tongue
48 (Coats and Karnauskas 2017; Seager et al. 2019, 2022; Heede and Fedorov 2023). Observations
49 stand in conflict with arguments based on air-sea flux scalings, which indicate that the cold
50 tongue should warm at an accelerated rate under greenhouse gas forcing (Knutson and Manabe
51 1995; Xie et al. 2010). Likewise, model projections suggest that increased low-level moisture
52 under global warming should weaken the Walker circulation and reduce wind-driven equatorial
53 upwelling (Vecchi et al. 2006; Vecchi and Soden 2007). Discrepancy between historical SST trends
54 and atmospheric arguments suggest that the observed cooling is influenced by subsurface ocean
55 processes (Clement et al. 1996; Kang et al. 2023; Hwang et al. 2024; Zhuo et al. 2024). Naturally,

56 theories seeking to explain historical cooling invoke changes in equatorial upwelling and its effect
57 on SST. Typically, these theories are split in two fundamental ways:

- 58 • Are climate models failing to cool the cold tongue because they upwell waters that are
59 unrealistically warm, or because upwelling velocities are too slow?
- 60 • Are the sources of model errors relevant to the SST trend discrepancy contained in the near-
61 equatorial region, or do errors originate in the subtropics? (Seager et al. 2019; Kang et al.
62 2023; Hwang et al. 2024)

63 It is likely that processes leading to widespread model errors are both thermal and dynamical,
64 equatorial and off-equatorial (Heede and Fedorov 2021). However, bridging the gaps between ex-
65 isting theories is complicated because ECS- and STC- based explanations of equatorial upwelling
66 are so distinct from each other. Moreover, the perception that equatorial upwelling is ‘pulled from
67 above’ by equatorial easterly winds overwhelmingly dominates scientists’ understanding of equa-
68 torial upwelling. Because dynamical understanding of this matter is based on mass conservation
69 rather than vertical forces, it remains unclear whether upwelling can indeed be ‘pushed from be-
70 low,’ as is necessary to support claims by Kleeman et al. (1999). As a result, our understanding of
71 equatorial upwelling lacks the precision and adaptability necessary to bridge ECS- and STC-based
72 theories of Pacific variability. Ultimately, this prevents progress in explaining observed historical
73 cooling in the cold tongue.

74 Previous studies have used available energetics analyses to simplify equatorial Pacific Ocean
75 dynamics. Particular focus has been given to the relation between mechanical wind work and
76 gravitational potential energy storage in the thermocline (Fedorov 2002; Brown and Fedorov
77 2008, 2010). Without precise energy conservation laws, however, such studies have mostly used
78 energetics to describe well-known dynamics and reduce their dimensionality (Shi et al. 2020). In
79 particular, note that the aforementioned studies only refer to basin-integrated energy, much like
80 Lorenz (1955) and Oort et al. (1994) did for the global atmosphere and ocean respectively. Without
81 locally-defined energy balances, the explanatory power of ocean energetics studies is drastically
82 limited.

83 Here, we use a locally-defined framework of available energetics with complete conservation
84 laws (Tailleux 2013) to trace back the energy sources that power equatorial Pacific upwelling.

By separating the contributions of kinetic and available potential energy reservoirs, we find that 20-50% of equatorial upwelling cannot be powered directly by winds along the equator, as usually understood, and instead relies on the energy of equatorward thermocline flows. We trace the majority of this energy to meridional overturning in the near-equatorial cells that downwell within 10°S and 10°N. Diabatic heating and downwelling across the STCs supply additional energy. Our findings provide a dynamical basis for the notion that equatorial upwelling can be regulated by a push from below. The framework presented here can help evaluate the ocean response to complex changes in the Walker circulation and facilitate the comparison of ECS- and STC-based theories of climate variability on interannual and decadal timescales alike.

2. Energetic Framework of Upwelling

Available potential energy in a stratified fluid quantifies the amount of work that can be extracted by adiabatic redistributions of fluid parcels (Lorenz 1955). This energy is usually partitioned into internal and gravitational potential energy reservoirs; to define these, one needs to consider the difference in net gravitational potential energy between a fluid’s actual density field ($\rho = \rho(\mathbf{x}, t)$, where $\mathbf{x} = (x, y, z)$) and a hypothetical reference state $\rho_r(z, t)$ (Holliday and McIntyre 1981). Here, we consider equations of state under which density of seawater is determined by conservative temperature Θ , salinity S , and pressure p such that $\rho(\mathbf{x}, t) = \rho[\Theta(\mathbf{x}, t), S(\mathbf{x}, t), p(\mathbf{x}, t)]$.

There is no absolute ‘right’ way to derive ρ_r (Tailleux 2018), but convention is that ρ_r should i) result from adiabatic rearrangement of fluid parcels within the fluid volume V_r , and ii) approximate the fluid’s state of minimum net gravitational energy, with isopycnals laying flat and stably stratified. Preserving time dependence in ρ_r allows to transparently account for changes in the fluid thermodynamics that are caused by irreversible mixing as well as energy or mass fluxes across the boundaries of V_r (Winters et al. 1995; Huang 1998). Given ρ_r , one can assign a reference level $z_r = z_r(\mathbf{x}, t)$ to approximate the level of neutral buoyancy where a fluid parcel whose actual position is \mathbf{x} would reside in the adiabatically rearranged fluid (Tailleux 2013; Scotti and White 2014). Thus, we seek a solution $z_r(\mathbf{x}, t)$ that meets the condition

$$\rho[S(\mathbf{x}, t), \Theta(\mathbf{x}, t), p_0(z_r)] = \rho_r[z_r(\mathbf{x}, t), t]. \quad (1)$$

Dependence on $S(\mathbf{x}, t)$ and $\Theta(\mathbf{x}, t)$ in Eq. (1) implies that seawater properties are preserved as the water parcel is virtually moved between z and z_r . The energetics involved in such movements are thus reversible and quantified using z positive upwards. Yet, we account for the parcel's changing density as it moves between the Boussinesq pressures $p_0(z) = -\rho_0 g z$ and $p_0(z_r) = -\rho_0 g z_r$ (pink shading in Fig. 1), where g is gravity and $\rho_0 = 1024 \text{ kg m}^{-3}$. The local available gravitational potential energy density ($E_a(\mathbf{x}, t)$) thus quantifies the amount of work that can be extracted from moving a water parcel away from its current position z and to its reference level z_r . Conversely, positive work is needed to move a water parcel away from z_r , much like stretching or compressing a spring away from its equilibrium position. In fact, for quasigeostrophic flow one can write

$$E_a(\mathbf{x}, t) \approx N_r^2 (z - z_r)^2 / 2, \quad (2)$$

which is exactly the potential energy of a spring with the elastic constant $N_r^2 = -\frac{g}{\rho_0} \frac{\partial \rho_r}{\partial z}$ and equilibrium position z_r . As for a spring, E_a is definite positive and its sign does not distinguish between downward and upward displacements of fluid parcels. Rather, E_a quantifies the energy associated with deviations from ρ_r (Holliday and McIntyre 1981).

Precise treatment of E_a and its conservation laws is needed to account for diabatic effects and complex stratification profiles (Huang 1998; Kang and Fringer 2010; Scotti and White 2014). While the quasigeostrophic approximation in Eq. (2) has been used to study equatorial Pacific dynamics before (Brown and Fedorov 2008, 2010; Brown et al. 2011), there is important evidence that this approximation is not suitable for various ocean regions (Von Storch et al. 2012). More recently, local energetics frameworks with greater precision have been applied to study global and regional ocean energetics over a variety of timescales (Zemskova et al. 2015; Hochet et al. 2022). Here, we use the Boussinesq statement of local available energetics for diabatic compressible fluids laid out by Tailleux (2013, 2018). Given ρ_r and the density $\rho(\mathbf{x}, t)$ of a fluid parcel, this framework defines E_a using Eq. (3). A schematic in Fig. 1 uses gray and pink shading to represent the integral in this formulation.

$$E_a(\mathbf{x}, t) = \frac{g}{\rho_0} \int_{z_r}^z (\rho[S(\mathbf{x}, t), \Theta(\mathbf{x}, t), p_0(z')] - \rho_r(z', t)) dz'. \quad (3)$$

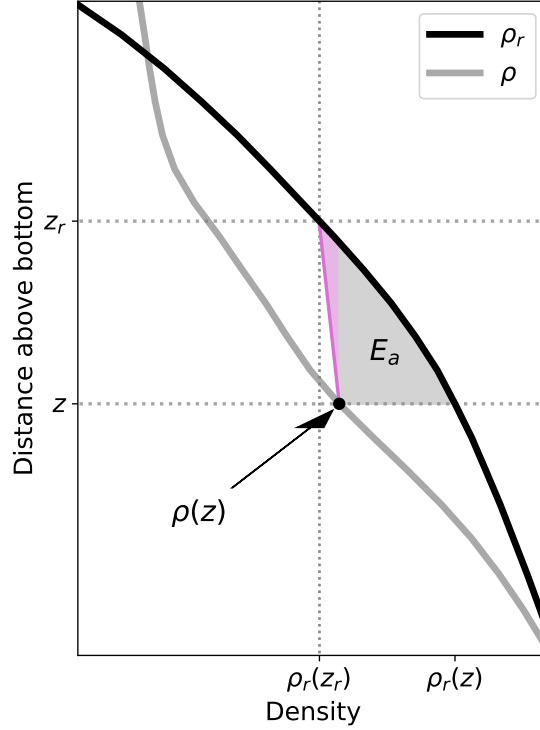


FIG. 1. Schematic explanation of E_a as defined in Eq. (3). Given the in-situ density profile ρ (gray line) and the fluid's ρ_r (black line), E_a evaluated at z is proportional to the shaded areas in gray and pink. Pink shading represents the effect of compressibility, as the diagonal pink line shows the change in ρ due to adiabatic expansion of a water parcel that moves between pressure levels at z and z_r .

The density difference that makes up the integrand of Eq. (3) captures the relative buoyancy that a water parcel would experience as it moves from z_r to z . Changes in density due to compressibility as the water parcel moves vertically are preserved in Eq. (3) and represented by pink shading in Fig. 1. In turn, gray shading in Fig. 1 represents the density difference between the parcel's density $\rho(\mathbf{x}, t)$ at its actual position \mathbf{x} and ρ_r . Given this, the conservation laws for E_a (Tailleux 2013; Saenz et al. 2015) and the local kinetic energy per unit mass ($E_k = (u^2 + v^2)/2$) of a hydrostatic fluid with the three-dimensional velocity ($\mathbf{u} = (u, v, w)$) are

$$\rho \frac{\partial}{\partial t} E_k = -\rho \mathbf{u} \cdot \nabla E_k - \nabla \cdot [\mathbf{u}(p - p_r)] - \rho' g w + \rho \mathbf{F}_h \cdot \mathbf{u} - \varepsilon, \quad (4)$$

and

$$\rho \frac{\partial E_a}{\partial t} = -\rho \mathbf{u} \cdot \nabla E_a + \rho' g w + \rho \dot{E}_a + \gamma, \quad (5)$$

where

$$\rho'(\mathbf{x}, t) = \rho(\mathbf{x}, t) - \rho_r(z, t). \quad (6)$$

Ordered as they appear, terms on the right hand side of Eq. (4) represent advection, pressure work, the rate of energy transfer from E_k into E_a , viscous work (with $\mathbf{F}_h = (F_x, F_y, 0)$ representing a horizontal viscous force vector that includes the wind stress), as well as dissipation and compressive terms that are grouped into ε and will not be considered in calculations below given their relatively small magnitude. Similarly, terms in the right hand side of Eq. (5) represent advection, energy conversions from E_k , diabatic changes to E_a (written as \dot{E}_a), and non-local effects (γ) that will not be further considered here.

a. Energy transfers between E_k and E_a

Notice that the term $\rho'gw$ appears with opposite signs in Eqs. (4) and (5), thus representing a transfer of energy between E_k and E_a . We henceforth refer to these energy conversions as $E_k \rightarrow E_a$ and $E_a \rightarrow E_k$, depending on the direction of energy transfer. When $\rho'gw > 0$, E_k is used to move water parcels away from their z_r and thus increase E_a , much like when we stretch or compress a spring ($E_k \rightarrow E_a$). In contrast, when $\rho'gw < 0$, energy stored in E_a is transformed into E_k as motion brings water parcels closer to their respective z_r ($E_a \rightarrow E_k$). We put particular focus on this term $\rho'gw$ that quantifies reversible energy transfers between E_k and E_a because it isolates w and thus points to the energetic implications of upwelling.

Energy transfers $\rho'gw$ in upwelling regions ($w > 0$) may flow in either direction between E_k and E_a . This is profoundly consequential because it means that upwelling may be powered by either E_k or E_a . Given the sign of w , the direction of local energy flows is thus determined by the sign of ρ' , and vice versa.

At locations \mathbf{x} where $\rho' < 0$, upwelling can be powered by E_a because the water parcel at \mathbf{x} is located at a depth greater than its reference level (i.e. $z < z_r$). This means that buoyancy forces implied by $\rho' < 0$ help the water parcel accelerate upwards and upwelling can occur without additional E_k input. In such situations, we refer to the water parcel as ‘light,’ which is relative to both the parcel’s ρ , its actual level z , and ρ_r . In contrast, when $\rho' > 0$, we refer to water parcels as ‘heavy,’ because they are located above their z_r ($z > z_r$). Upward movement of such water parcels thus requires additional E_k input that is transferred into the local E_a at a rate $\rho'gw > 0$. On

the flipside, downwelling ($w < 0$) of ‘light’ ($\rho' < 0$) water requires additional E_k input, while E_a powers the same motion for a ‘heavy’ ($\rho' > 0$) water parcel.

Interpretation of the balances between $\rho'gw$ and other terms in Eqs. (4) and (5) ultimately lead to a detailed picture of the drivers and energetics of vertical motion. Even though the numerical values of each term depend on the choice of ρ_r , the energy conservation laws are exact despite this choice, and numerical sensitivity is easily testable as shown in Section 3c (Wong et al. 2016; Tailleux 2018).

The words ‘light’ and ‘heavy’ associated with the sign of ρ' may remind some readers of energy conversions associated with static instabilities. However, conversions of E_a into E_k described here can happen in a fluid that remains stably stratified everywhere (Turner 1969). Rather, the vertical motions that concern us typically happen when ‘light’ and ‘heavy’ fluid occupy the same vertical level and are rearranged by both vertical and horizontal motions.

In a hydrostatic fluid, whose vertical momentum equation does not include w , one cannot easily relate vertical motion to vertical forces. In energetics, buoyancy ρ' takes the place of such force, but the energy that powers vertical motion is supplied by pressure work, which yields the term $\rho'gw$ in the E_k equation Gregory and Tailleux (2011); Saenz et al. (2015). Gravity currents and baroclinic instability help exemplify this particularly well; as lateral gradients drive high- ρ parcels forward against low- ρ ones, the low- ρ parcels ascend and allow denser parcels to spread out across the bottom of the fluid volume. Thus, vertical motion emerges from lateral gradients in a fluid without requiring that the fluid is ever unstably stratified (Lorenz 1955).

195 *b. Diabatic changes to E_a*

Reversible changes to E_a occur through adiabatic rearrangements of water parcels that change z and thus modify the displacement ($z - z_r$). In contrast, irreversible changes \dot{E}_a result from diabatic transformations of seawater properties Θ and S , which change a water parcel’s ρ and thus redefine its z_r (Eq. 1). For example, a ‘heavy’ ($z > z_r$, $\rho' > 0$) water parcel can lose its E_a when heat is added or S removed diabatically to reduce ρ and lift up z_r . Conversely, a ‘light’ ($z < z_r$, $\rho' < 0$) water parcel can lose its E_a when its ρ is diabatically increased and z_r lowered. Following Tailleux (2013), we account for these effects in Eq. (5) through the term

$$\rho \dot{E}_a(\mathbf{x}, t) = g \left[\frac{D\Theta}{Dt} \int_{z_r}^z \frac{\partial \rho}{\partial \Theta} dz' + \frac{DS}{Dt} \int_{z_r}^z \frac{\partial \rho}{\partial S} dz' \right], \quad (7)$$

where $\frac{D\Theta}{Dt}$ and $\frac{DS}{Dt}$ are the material derivatives of Θ and S . These terms are set by diabatic changes in temperature and salinity respectively, which result from air-sea fluxes and ocean turbulence. Likewise, the integrands $\frac{\partial \rho}{\partial \Theta}$ and $\frac{\partial \rho}{\partial S}$ represent the partial derivatives of density with Θ and S , and are proportional to thermal expansion and haline contraction coefficients.

c. Implementation on CESM2

We used output from fully coupled historical simulations of CESM2 (Danabasoglu et al. 2020) to compute individual terms in Eqs. (4) and (5). A model, rather than a reanalysis product, is used here because the latter don't typically conserve energy. Furthermore, using a brand-new model simulation allows us to precisely estimate terms in Eq. (7) that cannot be extracted from publicly available datasets. Even though CESM2 has many biases when compared to oceanographic observations, it is energetically and physically consistent. Thus, an ocean model can best help us leverage the precise conservation laws in Eqs. (5) and (4).

Model output was saved as monthly averages and on the standard CESM2 ocean grid, which has a nominal resolution 1 degree but reaches meridional spacings of 0.27 degrees at the Equator (Danabasoglu et al. 2020). To minimize the effects of transient eddies, all estimates shown below are computed from yearly-averaged quantities for the period between 1950 and 2010, unless noted otherwise. For example, E_a is estimated using yearly-averaged values of ρ and the reference state ρ_r corresponding to that year. Advective terms $\mathbf{u} \cdot \nabla E_a$ are then computed with yearly-averaged values of \mathbf{u} . One exception is in Section 3b, where composites of equatorial energetics during El Niño and La Niña were computed using monthly values of ρ , \mathbf{u} , and ρ_r . As we detail in Section 3, yearly-averaged values can approximately close the mean E_a budget in the western Pacific thermocline, which is our primary focus. However, eddies and the seasonal cycle appear to play a greater role in other regions, and this will be the subject of future work.

Some aspects of our results are sensitive to the choice of the fluid volume V_r , which sets ρ_r . V_r was defined as the Pacific Ocean between 35°S and 35°N, from the surface to 800 m depth. This corresponds roughly to latitudinal extent occupied by the STCs. We chose this area because our

focus is on understanding energetic interactions between the ECS and STCs. More details on the sensitivity of our results to the choice of V_r are given in Section 3b.

Given V_r , we computed time-dependent profiles of ρ_r by rearranging water parcels across V_r for both monthly- and yearly-averaged output. To do so, we binned the surface potential density σ_0 in 0.125 kg m^{-3} increments for all grid cells across V_r . We then estimated the total volume of seawater in each density class and allocated water masses to different reference depths z_r while constraining the amount of volume available at each level. Numerically, this was achieved by relating cumulative density functions of σ_0 and of the distribution of volume available for seawater storage across V_r as a function of z_r (Tseng and Ferziger 2001). Once sorted, we used a linear compressibility coefficient to approximate the effect of pressure as parcels were converted from σ_0 back into ρ . This method is roughly equivalent to the surface-to-bottom, volume-frequency approach tested in Saenz et al. (2015), with the exception that our approach is based on σ_0 and does not preserve the full distinct effects of Θ and S on ρ_r .

The diabatic term $\rho \dot{E}_a$ was computed using Eq. (7) with $D\Theta/Dt = \frac{\partial \Theta}{\partial t} + \mathbf{u} \cdot \nabla \Theta$ and $DS/Dt = \frac{\partial S}{\partial t} + \mathbf{u} \cdot \nabla S$ computed as the material derivatives of Θ and S . This can be equated to diabatic changes because both Θ and S are materially-conserved quantities. CESM2 outputs monthly-averaged values of these tendencies under variable names TEND-TEMP, TEND-SALT, TOT-ADV-TEMP, and TOT-ADV-SALT. Seawater properties including the dependence of σ_0 on Θ and S , linear compressibility coefficients, and integrands in Eq. (7) were computed using the Gibbs SeaWater Toolbox (McDougall and Barker 2011).

3. Results

The tilt of the equatorial thermocline produces a zonal contrast in ρ' , with a region of light ($\rho' < 0$) water that is mostly west of 220°E and heavy ($\rho' > 0$) water east of 220°E (Fig. 2). Values of $z_r - z > 0$ indicate vertical displacements that can be powered by E_a without additional energy inputs, ranging between 60 and -100 m across the equatorial Pacific (Figs. 2c,d). As we show below, equatorial upwelling in regions where $z_r - z > 0$ ($\rho' < 0$) is powered by E_a , implying that E_k supplied by local winds cannot directly sustain that fraction of equatorial upwelling.

Equatorial upwelling is powered by both E_k and E_a . The zonal tilt in the equatorial thermocline makes it such that ‘light’ water with $\rho' < 0$ covers much of the equatorial Pacific thermocline

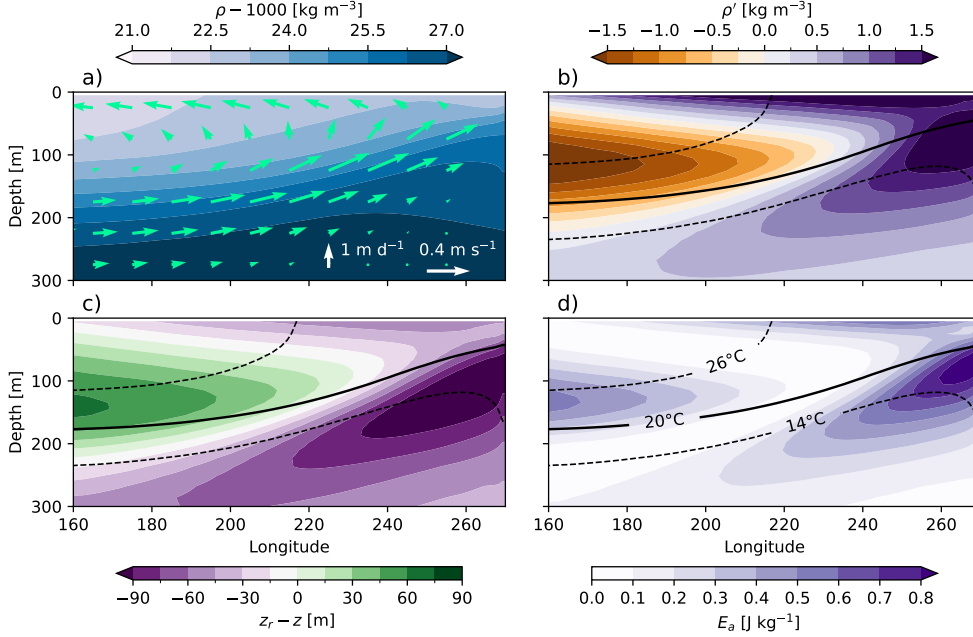


FIG. 2. Mean state of potential energy in the equatorial Pacific (3°S, 3°N). Color shading shows a) ρ , b) ρ' , c) $z - z_r$, and d) E_a , while green arrows in a) show the mean velocities (u, w) with w magnified for clarity. White arrows in a) show the scale of vectors in each direction. Black contours in c-d) show the mean positions of the 14, 20, and 26°C isotherms.

between 160°E and 220°E. Therefore, water masses here move closer to their z_r as they move up and eastward along the Equatorial Undercurrent (EUC). This results in $\rho'gw < 0$ and implies energy conversions $E_a \rightarrow E_k$ (blue shading in Fig. 3a). In contrast, upwelling of ‘heavy’ water east of 220°E incurs a conversion $E_k \rightarrow E_a$ (red shading in Fig. 3a). Closing the energetic balance of equatorial upwelling thus requires that we find sources of E_a west of 220°E but sources of E_k to the east. In areas where $\rho'gw > 0$, we may point to the wind stress \mathbf{F} as the energy source that explains upwelling (Eq. 4).

Advection of E_a into the equatorial Pacific thermocline supplies most of the energy necessary to drive upwelling west of 220°E (Fig. 3b). Simultaneously, diabatic processes that include vertical and horizontal mixing supply additional E_a at shallower levels (Fig. 3c). Altogether, the sum $\rho\mathbf{u} \cdot \nabla E_a - \rho\dot{E}_a$ can continuously supply the E_a necessary to lift thermocline water parcels west of 200°E by ~ 40 m or more (Figs. 2c, 3). This supports the view in Kleeman et al. (1999) that equatorial upwelling can be pushed from below.

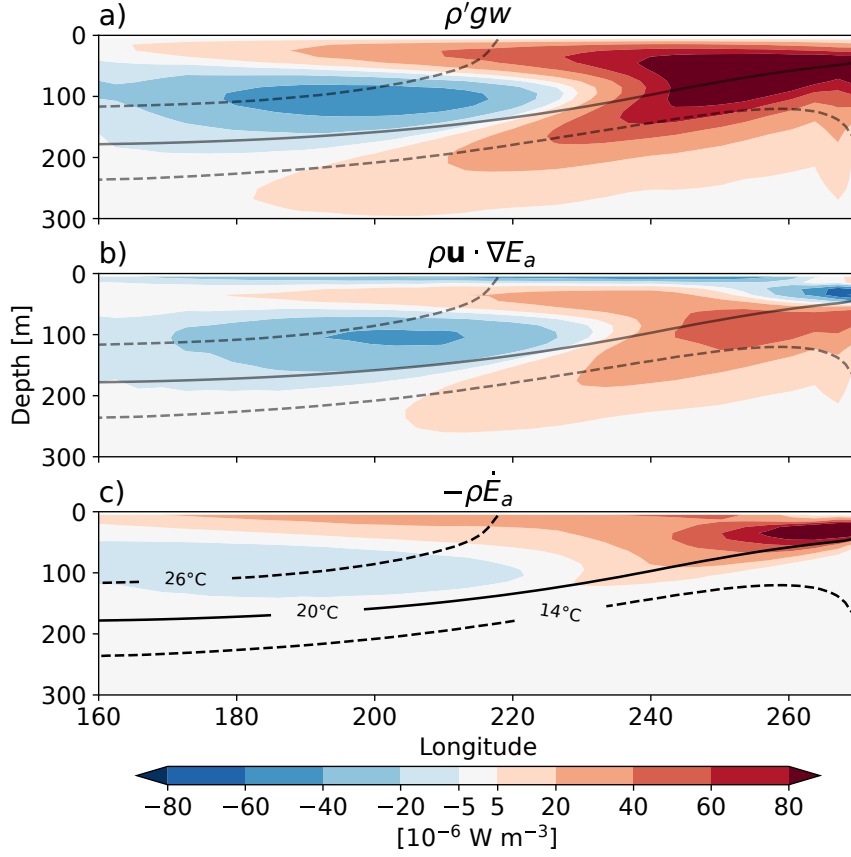


FIG. 3. Energetic balance of equatorial upwelling. Temporal averages of a) $\rho'gw$, b) $\rho\mathbf{u} \cdot \nabla E_a$, and c) $-\rho\dot{E}_a$ using yearly output from a historical CESM2 run. All values are averaged between 3°S and 3°N . The thermocline follows the approximate balance $\rho'gw \approx \rho\mathbf{u} \cdot \nabla E_a - \rho\dot{E}_a$ (Fig. S2).

a. Sources of E_a

Let us now turn our attention to Eq. (5) in search of sources of E_a and mechanisms that may transport energy into areas where $\rho'gw < 0$ (Fig. 3a). Sources of E_a exist wherever the absolute difference $\|z - z_r\|$ of a given water parcel increases over time. Namely, wherever

- ‘heavy’ ($\rho' > 0$) water moves upward ($w > 0$),
- ‘light’ ($\rho' < 0$) water moves downward ($w < 0$),
- diabatic changes to temperature or salinity quantified by $D\Theta/Dt$ and DS/Dt move a water parcel’s z_r farther away from its actual position z .

Vertical integrals of $\rho'gw$ across the STCs (Fig. 4) highlight areas where reversible energy conversions $E_k \rightarrow E_a$ (red shading) and $E_a \rightarrow E_k$ (blue shading) take place. Vertical integrals of advective and diabatic effects in Fig. 5 help understand how the E_a that results from conversions $E_k \rightarrow E_a$ is redistributed and modified by atmospheric heating and parameterized ocean processes. Together, these terms help sustain the mean distribution of E_a across the Pacific Ocean. Notice, however, that the full effects of ocean eddies and other transient phenomena are not resolved by our estimates, which are based on yearly-averaged data.

Downwelling branches of the near-equatorial overturning cells are the primary supplier of E_a to the western equatorial thermocline. Wind-driven downwelling of ‘light’ waters converts $E_k \rightarrow E_a$ at rates $\sim 5 \times 10^{-3} \text{ W m}^{-2}$ directly north and south of the equatorial western Pacific (Figs. 4a). Patterns in $\rho \mathbf{u} \cdot \nabla E_a > 0$ in Fig. 5a show that mean ocean currents transport E_a from off-equatorial regions of downwelling and towards the equator, where it converges at rates $8 \times 10^{-3} \text{ W m}^{-2}$ and helps drive upwelling along the EUC (Figs. 7a, 4b). This energetic link between branches of the near-equatorial shallow overturning cell is further evidenced by two large reservoirs of E_a that flank the equatorial thermocline near 5°S and 5°N (Fig. 6a).

The diabatic contribution to E_a -driven upwelling in the western equatorial Pacific also originates largely from E_a reservoirs in the off-equatorial thermocline (5b). As parameterized processes warm the subsurface western equatorial Pacific (Fig. S3), they raise the z_r of water parcels and allow them to flow farther along the tilted thermocline without additional E_k sources. Ultimately, Figs. 4a,b, 5a,c, and 6a show that the downwelling branches of the near-equatorial overturning cells help power thermocline upwelling in the western equatorial Pacific (Fig. 6a). Additional sources of E_a exist in the northern western tropical Pacific and are largely balanced by advection, which may transport excess E_a to the equator or extratropics via the Mindanao and Kuroshio western boundary currents.

Equatorial upwelling east of 220°E implies a fundamentally different set of energy transfers. When flowing up and eastward along the EUC, water parcels coming from the western Pacific eventually reach their own z_r and thus exhaust their E_a . This means that continuing ascent towards the surface cold tongue requires a source of E_k to sustain the conversion $E_k \rightarrow E_a$ that covers much of the equator in Fig. 4c. This is where viscous work by winds may supply E_k and directly power upwelling. Conversions $E_k \rightarrow E_a$ here are partly balanced by mean advection away from

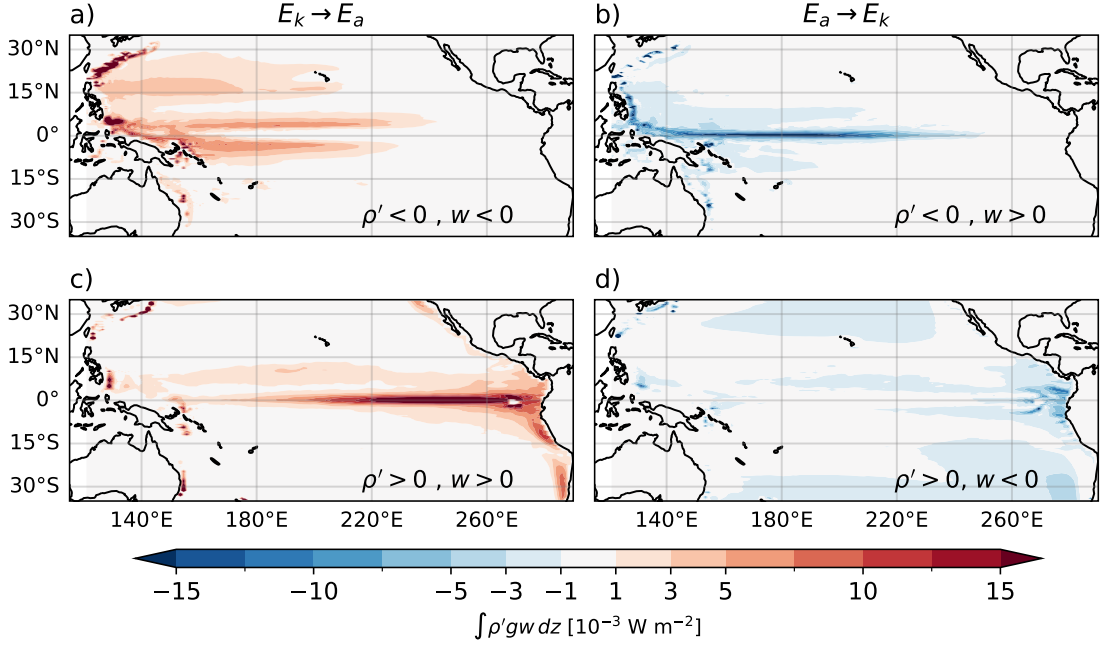


FIG. 4. Vertical integrals $\int \rho' g w dz$ between the surface and 500 m depth reveal reversible energy conversions (left column) $E_k \rightarrow E_a$ and (right column) $E_a \rightarrow E_k$. The signs of ρ' and w are separated to highlight energy conversions caused by a), d) downwelling, and by b), c) upwelling.

the equator and atmospheric heating. The divergent near-surface flow removes $> 15 \times 10^{-3} \text{ W m}^{-2}$ from parts of the equatorial cold tongue (Fig. 5a). Diabatic heating makes a far greater contribution to reducing E_a , as it lowers the density of near-surface water parcels and raises their z_r closer to the surface (Fig. 5c).

Volume integrals of terms in Eq. (5) help summarize estimates of E_a conversion, advection, and diabatic modification described above. Negative values of $\int_V \rho \mathbf{u} \cdot \nabla E_a dV$ and $\int_V \rho' g w dV$ in Fig. 6b depict the western side of the equatorial Pacific (blue bars) as an importer and user of E_a , whereas the eastern side (red bars) produces and exports E_a . The northern and southern sectors of the Pacific subtropical cells also contrast with each other, with the northern portion (green bars) advects E_a in, but also produces it. In contrast, the South Pacific (yellow bars) mean circulation yields negligible advective exchanges and reversible conversions of E_a . Instead, the South Pacific appears to balance a large net supply of E_a by transient phenomena that is largely canceled by diabatic transformations. Transient phenomena appear to export and use E_a in the eastern and northern Pacific sectors, and play a negligible role in the western equatorial Pacific.

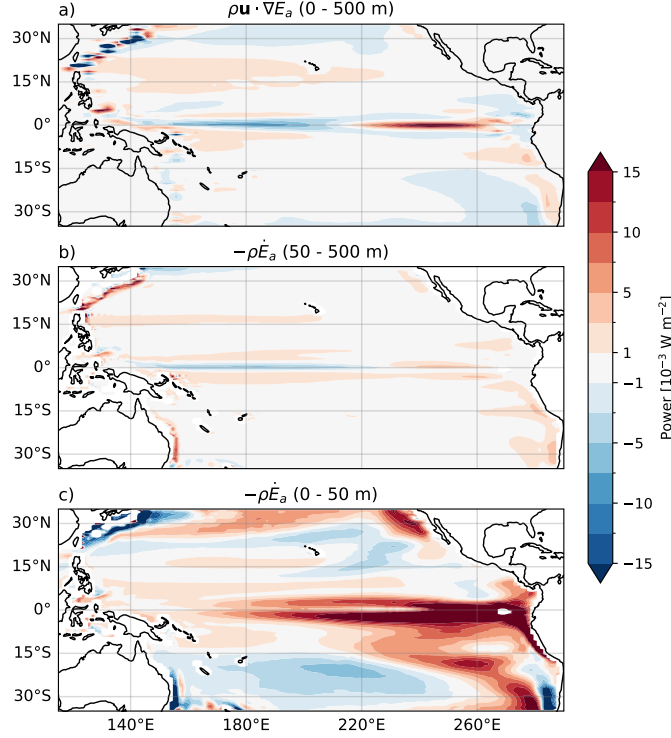


FIG. 5. Vertical integrals of a) advective and b-c) diabatic terms in Eq. (5). a) Three-dimensional advection is integrated over the top 500 m. Diabatic contributions $-\rho \dot{E}_a$ are shown separately for the b) top 50 m, and c) between 50 and 500 m depth. Patterns of \dot{E}_a are almost entirely explained by $D\Theta/Dt$ (Fig. S3).

E_a -driven upwelling in the western equatorial thermocline would be impossible without diabatic heating of near-surface waters around the cold tongue (Fig. 5c). Near-surface, E_a -rich waters exported out of the eastern equatorial sector are located 30 to 60 m above their z_r (Fig. 2c). Diabatic heating is thus essential because it lifts their z_r towards the surface and ensures that a conversion $E_k \rightarrow E_a$ occurs when those water parcels enter downwelling regions. If water parcels preserved their density as they flowed out of the cold tongue and E_a exported out of the eastern equatorial Pacific was not diabatically reduced, surface waters with $\rho' \sim 1 \text{ kg m}^{-3}$ (Fig. 2b) would readily move downwards and cause conversions $E_a \rightarrow E_k$ in downwelling branches of the near-equatorial overturning cell. In this case, the near-equatorial thermocline would not renew its E_a reservoir and thermocline upwelling would eventually stop west of 220°E. Thus, a near-equatorial energy cycle emerges:

1. E_a is converted into E_k as water parcels upwell along the EUC between 160°E and 220°E (regions where $\rho'gw < 0$ in Figs. 3a, 4b)
2. E_k is used to drive upwelling east of 220°E. This increases the E_a of ‘heavy’ ($\rho' > 0$) water parcels that reach the surface cold tongue (Figs. 2b, 3a, 4c).
3. Diabatic heating reduces the density of surface waters as they flow out of the cold tongue, thus lifting their z_r , reducing their E_a , and anchoring water parcels to the surface (Fig. 5c)
4. Near-equatorial winds supply E_k to drive downwelling in the near-equatorial cells and create E_a reservoirs that flank the equator (Figs. 4a, 6a).
5. Recently-downwelled waters carrying excess E_a flow towards the equator and supply the energy necessary to drive thermocline upwelling between 160°E and 220°E (Figs. 3b, 5a), thus restarting the cycle.

So far, we’ve established that equatorial upwelling along the EUC is composed of two phases that imply conversions $E_a \leftrightarrow E_k$ and energy transfers with off-equatorial regions. Thermocline reservoirs of E_a poleward of 10°S and 10°N (Fig. 6a) may also exchange energy with the equatorial region. This is more likely for the northwestern Pacific, where the conversion $E_k \rightarrow E_a$ is caused by downwelling of ‘light’ water in the subtropical gyre south of 25°N (Fig. 4a). E_a stored in the northwestern Pacific thermocline can reach the equatorial cell via the Mindanao current and other equatorward flows (Fig. 6a). This expands the possible sources of E_a that powers upwelling in the western equatorial thermocline, as momentum and buoyancy forcing in the subtropical gyre will influence the rate of E_a transport into regions with $\rho'gw < 0$ in Fig. 3a.

b. Sensitivity to V_r and ρ_r

The magnitude and spatial extent of conversions $E_k \rightarrow E_a$ that may supply E_a to the equator depends on the control volume V_r chosen for analysis and the corresponding reference state ρ_r . Estimates shown above are based on profiles $\rho_r(z, t)$ that result from adiabatically rearranging Pacific Ocean water parcels between 35°S and 35°N. But when V_r grows poleward, ρ_r becomes denser and a greater fraction of the equatorial thermocline will acquire $\rho' < 0$. As a result, a greater supply of E_a from off-equatorial sources will be needed to sustain upwelling in the western equatorial Pacific (Fig. S4).

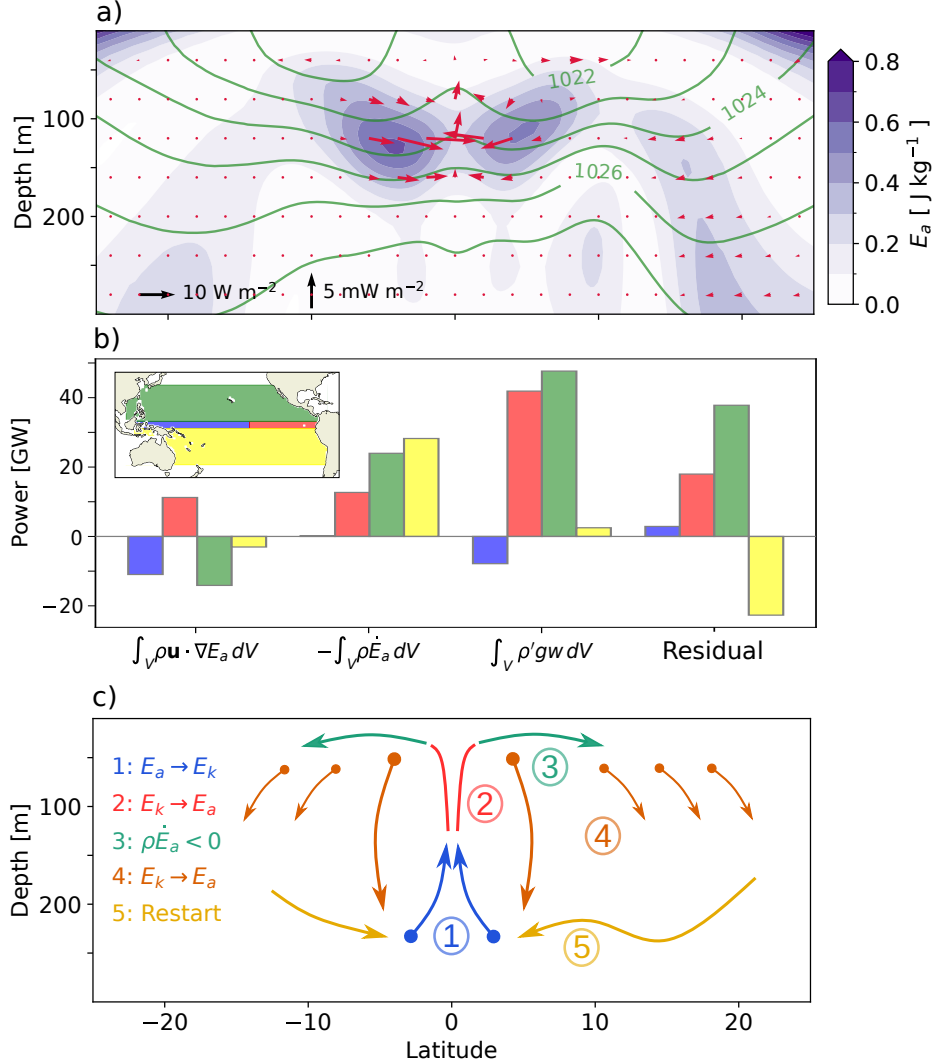


FIG. 6. Energetic links across the tropical Pacific. a) shows zonally-averaged E_a (shading), the meridional and vertical components of its transport $\mathbf{u}E_a$ (red arrows), and isopycnals (green contours) between 160°E and 220°E. b) shows volume averages of terms in Eq. (5) for four regions that are color-coded in the insert map. Residuals are calculated as $\int_V \rho' g w - \rho \mathbf{u} \cdot \nabla E_a + \rho \dot{E}_a dV$ and positive values imply that E_a must be exported or used by eddies or other transient phenomena. Blue and red regions split the equatorial Pacific at 220°E, while off-equatorial regions extend between 3° and 35° in each hemisphere. c) schematic representation of the energy cycle described in Section 3.1. Color-coded arrows and numbers refer to each step in that cycle, while the upper left legend indicates energy conversions and changes incurred by steps 1-4.

We now test the sensitivity of our results and constrain the degree to which equatorial upwelling relies on off-equatorial sources of E_a . To do this, we defined instances of V_r that extend across the

385 Pacific between variable limit latitudes ($\phi^\circ\text{S}$, $\phi^\circ\text{N}$), and down to 800 m depth. Given the profiles
 386 $\rho_r(z, t)$ that result from each choice of V_r , we estimated $\int_V \rho' g w dV$ and the ratio R in Eq. (8).
 387 This way, we obtain a range of values for the energetic cost of upwelling and the relative role of
 388 E_a sources under all conditions (Fig. 7).

389 As shown previously in Fig. 6b, $T(V) = \int_V \rho' g w dV$ yields the total E_k input necessary to sustain
 390 vertical motions within a volume V . It serves as a proxy for the local wind contribution to w , but
 391 does not explicitly distinguish it from other sources of E_k . To better understand the energetic links
 392 between equatorial and off-equatorial regions, Fig. 7a presents values of $T(V)$ for i) the Pacific
 393 equatorial region V_{EQ} , (between 3°S and 3°N , or the sum of blue and red areas in Fig. 6b) and ii)
 394 for the off-equatorial STC region $V_{STC} - V_{EQ}$ (between 35°S and 35°N but excluding V_{EQ} , or the
 395 sum of green and yellow areas in Fig. 6b).

396 Additionally, we estimate the energy ratio R (Eq. 8) and its dependence on V_r . R is defined only
 397 for V_{EQ} and yields the fraction of equatorial energy conversions that must be balanced by sources
 398 of E_a , rather than E_k . The numerator in Eq. (8) uses the Heaviside function $H(-\rho' g w)$ to account
 399 only for areas where conversions $E_a \rightarrow E_k$ occur, while the denominator accounts equally for all
 400 conversions $\rho' g w$ regardless of their sign.

$$R = \frac{\int_{V_{EQ}} |\rho' g w| H(-\rho' g w) dV}{\int_{V_{EQ}} |\rho' g w| dV} \quad (8)$$

401 Conversions $E_k \rightarrow E_a$ in each region vary with the choice of V_r and ρ_r , but changes in $T(V_{EQ})$ are
 402 largely compensated by $T(V_{STC} - V_{EQ})$ (Fig. 7a). As ϕ grows and V_r extends poleward, sustaining
 403 vertical motions in V_{EQ} requires that more E_a is imported and less E_k is used locally (Fig. 7b).
 404 As V_r extends beyond the tropics and ρ_r becomes denser, conversions $E_k \rightarrow E_a$ associated with
 405 wind-driven downwelling in $V_{STC} - V_{EQ}$ grow because the subtropical ocean is more likely to have
 406 $\rho' < 0$.

414 Despite drastic changes in the regional patterns of $\rho' g w$ for different choices of V_r , the total E_k
 415 input required to sustain vertical motions across the subtropical Pacific remains constant at roughly
 416 75 GW. This amounts to $\sim 15\%$ of the total wind work into the region (Fig. 7c). Therefore, rather
 417 than changing the net energetics implied by vertical motions, V_r and ρ_r determine whether E_k is
 418 spent subducting ‘light’ water into the thermocline or lifting ‘heavy’ parcels towards the surface.

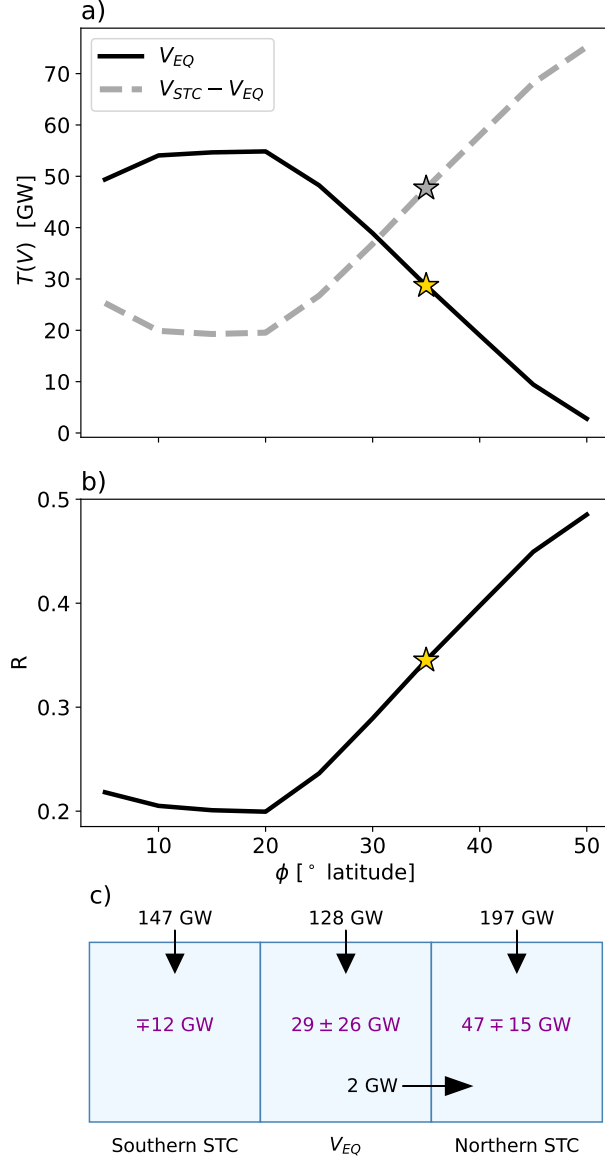


FIG. 7. Sensitivity of energy transfers to the latitudinal extent of V_r . a) the total E_k input needed to sustain vertical motions in the near-equatorial region (V_{EQ} , between 3°S and 3°N), and in the rest of the STCs ($V_{STC} - V_{EQ}$, from 35°S to 35°N excluding V_{EQ}). Stars indicate the value $\phi = 35^\circ$ used to produce all other figures in this study. c) is a schematic description of (black) E_k fluxes into V_{EQ} and the two regions that make up V_{STC} . Vertical arrows indicate windwork, and the horizontal arrow indicates fluxes by horizontal advection. The range of values $T(V)$ obtained from using $\phi \in [5^\circ, 50^\circ]$ is indicated in magenta. Advective fluxes less than 0.1 GW not shown.

419 With this, one cannot precisely estimate the degree to which equatorial upwelling is powered
420 directly by local winds.

421 Based on the sensitivity analysis in Fig. 7b, we assess that 20-50% of energy used by equatorial
422 upwelling must be supplied by off-equatorial sources of E_a . This is a lower bound for the
423 thermocline's energetic contribution to equatorial upwelling, since the thermocline could also
424 supply E_k to some equatorial regions where $\rho'gw > 0$ (Fig. 3a). Our analyses point to the
425 importance of energy exchanges between equatorial and off-equatorial regions (Fig. 6, 7a) via the
426 near-equatorial cells and the STCs alike. Based on these results and the fact that the STCs supply
427 the water masses that upwell along the EUC (Lu et al. 1998; Nie et al. 2019), we chose V_r to
428 span the Pacific from 35°S to 35°N and speculate that the thermocline's energetic contribution to
429 equatorial upwelling is closer to 50% than it is to 20%.

430 *c. Temporal variability*

431 Thermocline-driven upwelling is indirectly powered by the trade winds, as downwelling in the
432 edges of the near-equatorial cells imparts E_a onto subsurface waters that later reach the equator
433 (Figs. 4a, 6a). Thus, patterns of E_a across the tropical Pacific thermocline and its transport into the
434 equatorial region can help study forms of equatorial variability that are related to the trade winds.
435 Previous studies by Brown and Fedorov (2008, 2010) and Brown et al. (2011) have shown that
436 El Niño-Southern Oscillation (ENSO) can be represented as a cycle between trade wind strength
437 and the volume-integrated equatorial E_a . Here, we use the fact that conservation laws in Eqs. (4)
438 and (5) are locally valid and not only in a volume-integrated sense. To do so, we computed the El
439 Niño 3.4 index from our CESM2 runs and used monthly-averaged model output to create average
440 composites of the equatorial energy balance under El Niño and La Niña conditions (Fig. 8).

441 As noted by Brown and Fedorov (2008), E_a storage in the equatorial Pacific is intimately tied
442 to the zonal thermocline tilt (Figs. 2a,d). This tilt implies that water parcels in the west can
443 upwell without additional energy input ($z - z_r > 0$) while parcels in the east could readily downwell
444 ($z - z_r < 0$, Fig. 2c). The tilted thermocline and the E_a pattern it implies are sustained by E_k
445 input by winds. E_a west of 220°E is supplied by off-equatorial downwelling (Fig. 4a), while the
446 conversion $E_k \rightarrow E_a$ east of there can be powered by local winds along the equator (Fig. 4c).

When the winds weaken during El Niño events, conversions $E_k \rightarrow E_a$ decrease across the near-equatorial region and yields a weaker zonal thermocline tilt (Brown and Fedorov 2010; Brown et al. 2011). Simultaneously, the magnitude of $\rho \mathbf{u} \cdot \nabla E_a$ weakens and leads to reduced local E_a storage (Fig. 8a,b). A decrease in thermocline tilt is possible because E_a stored on each end of the basin can be used to drive upwelling where $\rho' < 0$ and downwelling where $\rho' > 0$ (Fig. 2c). As E_a is used by vertical motions and off-equatorial $E_k \rightarrow E_a$ weaken, equatorial E_a becomes depleted and buoyancy forces reach a new balance. The low- E_a state that characterizes El Niño events is directly opposite to the mechanisms that unfold during La Niña. When the trade winds strengthen, conversions $E_k \rightarrow E_a$ associated with both equatorial upwelling (Fig. 4c) and off-equatorial downwelling (Fig. 4a) increase. As a result, the thermocline tilt strengthens and equatorial E_a storage grows (Fig. 8c,d).

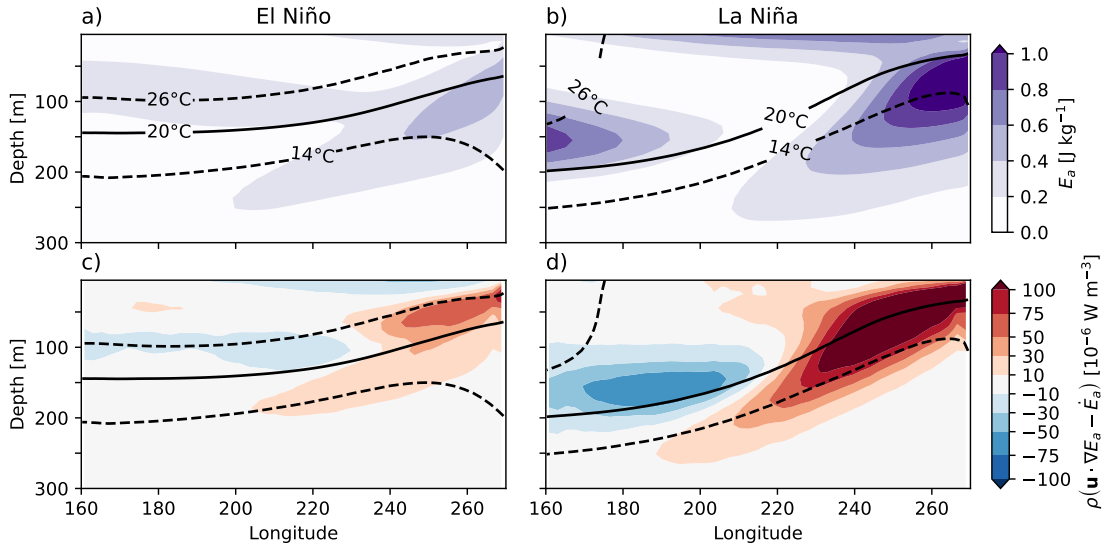


FIG. 8. Equatorial balance of E_a during El Niño (left column) and La Niña (right column). Color shading in a) and b) shows E_a , while shading in c) and d) shows $\rho \mathbf{u} \cdot \nabla E_a - \rho \dot{E}_a$, which is the sum of terms in Figs. 3b,c.

Contrast in E_a and $\rho \mathbf{u} \cdot \nabla E_a$ across the phases of ENSO are consistent with changes in upwelling that are crucial to ENSO theory (Fig. 8). Changes in the thermocline tilt enable redistribution of water masses that set the zonal SST gradient across the equatorial Pacific (Wyrtki 1975). Because the EUC flows eastward along the equatorial thermocline, an increased thermocline tilt implies a greater w , and Figs. 8c,d demonstrate that the subsurface supply of E_a to the equatorial thermocline

adjusts accordingly. With this, we see that E_a -driven upwelling is crucial not only to the mean state, but can also help understand equatorial variability.

4. Discussion

The notion that equatorial upwelling is partly ‘pushed from below’ may be surprising at first. However, it follows straightforwardly from conversions $E_k \rightarrow E_a$ caused by off-equatorial, wind-driven downwelling (Fig. 4a). As warm, low-density surface waters move down into the thermocline, they acquire $\rho' < 0$ and help sustain buoyancy forces that drive water upwards. This is an intrinsic feature of the equatorial cells and does not negate the claim in Wyrski (1981) that equatorial upwelling at the base of the mixed layer is proportional to the wind-driven Ekman divergence. Instead, our approach simply highlights the storage of thermocline E_a as a necessary intermediate step between Pacific wind forcing and upwelling along the EUC.

We find that energetic links between downwelling and upwelling branches of the near-equatorial overturning cells help sustain the tilt in the equatorial thermocline (Fig. 8). Bounded by regions of Ekman-driven downwelling that flank the equator, the cells were discovered long ago using hydrography (Cromwell 1953). The spatial structure of energy flows within the cells (Zemskova et al. 2015) and their relation to the broader Pacific Ocean (Lu et al. 1998) had been presented in previous studies. Still, their significance to coupled ocean-atmosphere dynamics seems to be underexplored. Results presented here may motivate scientists to further consider the dynamics of off-equatorial downwelling and its energetic interactions with surface heating and remote areas of the stratified ocean.

Quantifying the energetic contribution of thermocline buoyancy forces to equatorial upwelling helps clarify connections between the ECS and the STCs (Figs. 6, 7). Transfer of E_a from the STCs to the equator happens via mid-ocean equatorward flows (Fig. 6) and western boundary currents alike. The constant supply of E_a from off-equatorial sources ensures that water parcels in the western equatorial Pacific thermocline are able to upwell without additional energy inputs (Fig. 2c). When this supply weakens or strengthens during ENSO cycles, the equatorial thermocline releases or takes up more E_a and adjusts its tilt to match the changing conditions (Figs. 8).

Dynamical theories of equatorial upwelling have historically relied on mass balances to understand vertical motions (Wyrski 1981; Kleeman et al. 1999). In that sense, theories have focused on

ensuring consistency between horizontal forces and vertical velocities, rather than directly explaining the latter. The energetics framework described here may help formalize existing theories of equatorial upwelling, of its variability, and its connections to remote ocean conditions. Ultimately, evaluating the diversity of modeled equatorial Pacific responses to climate change requires that we find more satisfying explanations of upwelling velocities and that we learn to disentangle those from the thermodynamical implications of upwelling.

An important takeaway from our study is that thermal anomalies advected equatorward can change ρ in the Western Pacific and thus modify velocities w by modifying the advective supply of E_a (Figs. 3, 8). More intuitively, think that it takes more energy to lift cold, high-density water than it takes to lift low-density, warm water. This contrasts with the popular framework in which subtropical heating is thought to be advected passively into the equatorial cold tongue by an undisturbed circulation (Gu and Philander 1997). Future studies may use idealized modeling to test the extent to which density changes impact equatorial w under a fixed wind stress (Luongo et al. 2025).

Previous studies had analyzed the equatorial Pacific ocean from an available energetics perspective across multiple timescales (Fedorov 2002; Brown and Fedorov 2008, 2010; Brown et al. 2011; Shi et al. 2020). By adopting the more precise framework of available energetics formulated by Tailleux (2013, 2018), we are able to trace the sources of E_a that keep the equatorial thermocline tilted with upwelling along the EUC. This way, we find that E_a stored in the equatorial mean state (Fig. 2d) does not sit passively. Instead, our analysis shows that this E_a is actively used to power upwelling and replenished by low-density equatorward thermocline flows between 160°E and 220°E (Fig. 6).

Our analyses don't explicitly resolve the role of eddies and transient motions in the Pacific Ocean energetics. Residuals in Figs. 6b and S2 show that the mean circulation can largely close the E_a budget in the western equatorial Pacific but not elsewhere. Alternative frameworks of local energetics can help understand regions where eddies play a prominent role in shaping mean values of E_a (Scotti and White 2014; Tailleux and Rouillet 2025).

5. Conclusion

We used the Boussinesq local available energetics framework of Tailleux (2013, 2018) to detail the tropical thermocline's role in driving equatorial upwelling. Our analysis show that at least 20-50% of the energy involved in equatorial upwelling is supplied by the off-equatorial thermocline (Fig. 7b). This result follows from the low ρ of the western Pacific thermocline, which implies $\rho' < 0$ and thus allows 20-50% of the energy spent on equatorial upwelling to be supplied by E_a rather than E_k (Figs. 2, 3, 7). This implies that equatorial upwelling is partly pushed from below, and not only pulled from above, as intuition and mass balance arguments may suggest Wyrski (1981). This remote influence from below may help explain why equatorial upwelling has been observed in the presence of local westerly winds (Helber and Weisberg 2001).

We find evidence of a near-equatorial cycle involving vertical motions driven by both E_a and E_k , as well as diabatic changes to E_a caused by surface heating in the cold tongue (Fig. 6b). Reversible energy transfers that arise from vertical motions respond to variations in the trade winds and are thus in general agreement with classical theories of equatorial variability (Fig. 8). Our findings differ from common understanding, however, in that they establish a link between upwelling velocities and surface buoyancy fluxes. This link exists primarily because off-equatorial downwelling would not charge the thermocline with E_a if water parcels flowing out of the cold tongue preserved their ρ (Figs. 4a, 5a).

Lastly, we reiterate how our analyses point to near-equatorial downwelling as a crucial process helping control equatorial upwelling. Even though schematic depictions of the near-equatorial cells hint at a meaningful connection between equatorial and off-equatorial vertical motions (Lu et al. 1998), those links have lacked a dynamical basis beyond mass conservation. The analyses of local available energetics presented here may help better leverage connections between vertical motions across the tropical oceans in studies of global climate dynamics.

Acknowledgments. Without implying their endorsement, the authors are grateful for fruitful discussions with Rémi Tailleux, Feng Jiang, and Mark Cane. This work was funded by grant DE SC-0023333 from the US Department of Energy and grants AGS 22-17618 and OCE-2219829 from the National Science Foundation.

Data availability statement. Data and code used to produce the figures in this manuscript can be found in zenodo.org/records/13741896.

References

Brown, J. N., and A. V. Fedorov, 2008: Mean energy balance in the tropical pacific ocean. *Journal of Marine Research*, **66** (1), 1–23.

Brown, J. N., and A. V. Fedorov, 2010: How much energy is transferred from the winds to the thermocline on enso time scales? *Journal of Climate*, **23** (6), 1563–1580, <https://doi.org/doi.org/10.1175/2009JCLI2914.1>.

Brown, J. N., A. V. Fedorov, and E. Guilyardi, 2011: How well do coupled models replicate ocean energetics relevant to enso? *Climate Dynamics*, **36**, 2147–2158, <https://doi.org/doi.org/10.1007/s00382-010-0926-8>.

Capotondi, A., and Coauthors, 2023: Mechanisms of tropical pacific decadal variability. *Nature Reviews Earth & Environment*, **4** (11), 754–769, <https://doi.org/doi.org/10.1038/s43017-023-00486-x>.

Clement, A. C., R. Seager, M. A. Cane, and S. E. Zebiak, 1996: An ocean dynamical thermostat. *Journal of Climate*, **9** (9), 2190–2196, [https://doi.org/doi.org/10.1175/1520-0442\(1996\)009\(2190:AODT\)2.0.CO;2](https://doi.org/doi.org/10.1175/1520-0442(1996)009(2190:AODT)2.0.CO;2).

Coats, S., and K. Karnauskas, 2017: Are simulated and observed twentieth century tropical pacific sea surface temperature trends significant relative to internal variability? *Geophysical Research Letters*, **44** (19), 9928–9937, <https://doi.org/doi.org/10.1002/2017GL074622>.

Cromwell, T., 1953: Circulation in a meridional plane in the central equatorial pacific. *Journal of Marine Research*, **12** (2), 196–213.

- 571 Danabasoglu, G., and Coauthors, 2020: The community earth system model version 2 (cesm2).
572 *Journal of Advances in Modeling Earth Systems*, **12** (2), e2019MS001916, [https://doi.org/](https://doi.org/doi.org/10.1029/2019MS001916)
573 [doi.org/10.1029/2019MS001916](https://doi.org/doi.org/10.1029/2019MS001916).
- 574 Fedorov, A. V., 2002: The response of the coupled tropical ocean–atmosphere to westerly wind
575 bursts. *Quarterly Journal of the Royal Meteorological Society: A journal of the atmospheric*
576 *sciences, applied meteorology and physical oceanography*, **128** (579), 1–23, [https://doi.org/](https://doi.org/doi.org/10.1002/qj.200212857901)
577 [doi.org/10.1002/qj.200212857901](https://doi.org/doi.org/10.1002/qj.200212857901).
- 578 Gregory, J. M., and R. Tailleux, 2011: Kinetic energy analysis of the response of the atlantic
579 meridional overturning circulation to co2-forced climate change. *Climate dynamics*, **37**, 893–
580 914, <https://doi.org/doi.org/10.1007/s00382-010-0847-6>.
- 581 Gu, D., and S. G. Philander, 1997: Interdecadal climate fluctuations that depend on exchanges
582 between the tropics and extratropics. *Science*, **275** (5301), 805–807, [https://doi.org/doi.org/10.](https://doi.org/doi.org/10.1126/science.275.5301.805)
583 [1126/science.275.5301.805](https://doi.org/doi.org/10.1126/science.275.5301.805).
- 584 Heede, U. K., and A. V. Fedorov, 2021: Eastern equatorial pacific warming delayed by aerosols and
585 thermostat response to co2 increase. *Nature Climate Change*, **11** (8), 696–703, [https://doi.org/](https://doi.org/doi.org/10.1038/s41558-021-01101-x)
586 [doi.org/10.1038/s41558-021-01101-x](https://doi.org/doi.org/10.1038/s41558-021-01101-x).
- 587 Heede, U. K., and A. V. Fedorov, 2023: Colder eastern equatorial pacific and stronger walker
588 circulation in the early 21st century: Separating the forced response to global warming from
589 natural variability. *Geophysical Research Letters*, **50** (3), e2022GL101020, [https://doi.org/doi.](https://doi.org/doi.org/10.1029/2022GL101020)
590 [org/10.1029/2022GL101020](https://doi.org/doi.org/10.1029/2022GL101020).
- 591 Helber, R. W., and R. H. Weisberg, 2001: Equatorial upwelling in the western pacific warm pool.
592 *Journal of Geophysical Research: Oceans*, **106** (C5), 8989–9003, [https://doi.org/doi.org/10.](https://doi.org/doi.org/10.1029/2000JC000401)
593 [1029/2000JC000401](https://doi.org/doi.org/10.1029/2000JC000401).
- 594 Hochet, A., T. Huck, O. Arzel, F. Sévellec, and A. C. d. Verdière, 2022: Energy transfers between
595 multidecadal and turbulent variability. *Journal of Climate*, **35** (4), 1157–1178, [https://doi.org/](https://doi.org/doi.org/10.1175/JCLI-D-21-0136.1)
596 [doi.org/10.1175/JCLI-D-21-0136.1](https://doi.org/doi.org/10.1175/JCLI-D-21-0136.1).

Holliday, D., and M. E. McIntyre, 1981: On potential energy density in an incompressible, stratified fluid. *Journal of Fluid Mechanics*, **107**, 221–225, <https://doi.org/doi.org/10.1017/S0022112081001742>.

Huang, R. X., 1998: Mixing and available potential energy in a boussinesq ocean. *Journal of Physical Oceanography*, **28** (4), 669–678, [https://doi.org/doi.org/10.1175/1520-0485\(1998\)028<0669:MAAPEI>2.0.CO;2](https://doi.org/doi.org/10.1175/1520-0485(1998)028<0669:MAAPEI>2.0.CO;2).

Hwang, Y.-T., S.-P. Xie, P.-J. Chen, H.-Y. Tseng, and C. Deser, 2024: Contribution of anthropogenic aerosols to persistent la niña-like conditions in the early 21st century. *Proceedings of the National Academy of Sciences*, **121** (5), e2315124 121, <https://doi.org/doi.org/10.1073/pnas.2315124121>.

Kang, D., and O. Fringer, 2010: On the calculation of available potential energy in internal wave fields. *Journal of Physical Oceanography*, **40** (11), 2539–2545, <https://doi.org/doi.org/10.1175/2010JPO4497.1>.

Kang, S. M., P. Ceppi, Y. Yu, and I.-S. Kang, 2023: Recent global climate feedback controlled by southern ocean cooling. *Nature Geoscience*, **16** (9), 775–780, <https://doi.org/doi.org/10.1038/s41561-023-01256-6>.

Karnauskas, K. B., R. Seager, A. Kaplan, Y. Kushnir, and M. A. Cane, 2009: Observed strengthening of the zonal sea surface temperature gradient across the equatorial pacific ocean. *Journal of Climate*, **22** (16), 4316–4321, <https://doi.org/doi.org/10.1175/2009JCLI2936.1>.

Kleeman, R., J. P. McCreary Jr, and B. A. Klinger, 1999: A mechanism for generating enso decadal variability. *Geophysical Research Letters*, **26** (12), 1743–1746, <https://doi.org/doi.org/10.1029/1999GL900352>.

Knutson, T. R., and S. Manabe, 1995: Time-mean response over the tropical pacific to increased c02 in a coupled ocean-atmosphere model. *Journal of Climate*, **8** (9), 2181–2199, [https://doi.org/doi.org/10.1175/1520-0442\(1995\)008<2181:TMROTT>2.0.CO;2](https://doi.org/doi.org/10.1175/1520-0442(1995)008<2181:TMROTT>2.0.CO;2).

Lorenz, E. N., 1955: Available potential energy and the maintenance of the general circulation. *Tellus*, **7** (2), 157–167, <https://doi.org/doi.org/10.3402/tellusa.v7i2.8796>.

- Lu, P., J. P. McCreary Jr, and B. A. Klinger, 1998: Meridional circulation cells and the source waters of the pacific equatorial undercurrent. *Journal of Physical Oceanography*, **28** (1), 62–84, [https://doi.org/doi.org/10.1175/1520-0485\(1998\)028<0062:MCCATS>2.0.CO;2](https://doi.org/doi.org/10.1175/1520-0485(1998)028<0062:MCCATS>2.0.CO;2).
- Luo, J.-J., S. Masson, S. Behera, P. Delecluse, S. Gualdi, A. Navarra, and T. Yamagata, 2003: South pacific origin of the decadal enso-like variation as simulated by a coupled gcm. *Geophysical Research Letters*, **30** (24), <https://doi.org/doi.org/10.1029/2003GL018649>.
- Luongo, M. T., S.-P. Xie, I. Eisenman, S. Sun, and Q. Peng, 2025: How the subsurface tropical pacific responds to subtropical surface cooling: Implications for cross-equatorial transport. *Journal of Climate*, <https://doi.org/doi.org/10.1175/JCLI-D-24-0440.1>.
- McDougall, T. J., and P. M. Barker, 2011: Getting started with teos-10 and the gibbs seawater (gsw) oceanographic toolbox. *Scor/iapso WG*, **127** (532), 1–28.
- Nie, X., S. Gao, F. Wang, J. Chi, and T. Qu, 2019: Origins and pathways of the pacific equatorial undercurrent identified by a simulated adjoint tracer. *Journal of Geophysical Research: Oceans*, **124** (4), 2331–2347, <https://doi.org/doi.org/10.1029/2018JC014212>.
- Oort, A. H., L. A. Anderson, and J. P. Peixoto, 1994: Estimates of the energy cycle of the oceans. *Journal of Geophysical Research: Oceans*, **99** (C4), 7665–7688, <https://doi.org/doi.org/10.1029/93JC03556>.
- Saenz, J. A., R. Tailleux, E. D. Butler, G. O. Hughes, and K. I. Oliver, 2015: Estimating lorenz’s reference state in an ocean with a nonlinear equation of state for seawater. *Journal of Physical Oceanography*, **45** (5), 1242–1257, <https://doi.org/doi.org/10.1175/JPO-D-14-0105.1>.
- Scotti, A., and B. White, 2014: Diagnosing mixing in stratified turbulent flows with a locally defined available potential energy. *Journal of Fluid Mechanics*, **740**, 114–135, <https://doi.org/doi.org/10.1017/jfm.2013.643>.
- Seager, R., M. Cane, N. Henderson, D.-E. Lee, R. Abernathey, and H. Zhang, 2019: Strengthening tropical pacific zonal sea surface temperature gradient consistent with rising greenhouse gases. *Nature Climate Change*, **9** (7), 517–522, <https://doi.org/doi.org/10.1038/s41558-019-0505-x>.

Seager, R., N. Henderson, and M. Cane, 2022: Persistent discrepancies between observed and modeled trends in the tropical pacific ocean. *Journal of Climate*, **35** (14), 4571–4584, <https://doi.org/doi.org/10.1175/JCLI-D-21-0648.1>.

Shi, J., A. V. Fedorov, and S. Hu, 2020: A sea surface height perspective on el niño diversity, ocean energetics, and energy damping rates. *Geophysical Research Letters*, **47** (7), e2019GL086742, <https://doi.org/doi.org/10.1029/2019GL086742>.

Tailleux, R., 2013: Available potential energy density for a multicomponent boussinesq fluid with arbitrary nonlinear equation of state. *Journal of Fluid Mechanics*, **735**, 499–518, <https://doi.org/doi.org/10.1017/jfm.2013.509>.

Tailleux, R., 2018: Local available energetics of multicomponent compressible stratified fluids. *Journal of Fluid Mechanics*, **842**, R1, <https://doi.org/doi.org/10.1017/jfm.2018.196>.

Tailleux, R., and G. Rouillet, 2025: Energetically consistent localised ape budgets for local and regional studies of stratified flow energetics. *Ocean Modelling*, 102579, <https://doi.org/doi.org/10.1016/j.ocemod.2025.102579>.

Tseng, Y.-h., and J. H. Ferziger, 2001: Mixing and available potential energy in stratified flows. *Physics of Fluids*, **13** (5), 1281–1293, <https://doi.org/doi.org/10.1063/1.1358307>.

Turner, J., 1969: Buoyant plumes and thermals. *Annual Review of Fluid Mechanics*, **1** (1), 29–44, <https://doi.org/doi.org/10.1146/annurev.fl.01.010169.000333>.

Vecchi, G. A., and B. J. Soden, 2007: Global warming and the weakening of the tropical circulation. *Journal of Climate*, **20** (17), 4316–4340, <https://doi.org/doi.org/10.1175/JCLI4258.1>.

Vecchi, G. A., B. J. Soden, A. T. Wittenberg, I. M. Held, A. Leetmaa, and M. J. Harrison, 2006: Weakening of tropical pacific atmospheric circulation due to anthropogenic forcing. *Nature*, **441** (7089), 73–76, <https://doi.org/doi.org/10.1038/nature04744>.

Von Storch, J.-S., C. Eden, I. Fast, H. Haak, D. Hernández-Deckers, E. Maier-Reimer, J. Marotzke, and D. Stammer, 2012: An estimate of the lorenz energy cycle for the world ocean based on the storm/ncep simulation. *Journal of Physical Oceanography*, **42** (12), 2185–2205, <https://doi.org/https://doi.org/10.1175/JPO-D-12-079.1>.

Winters, K. B., P. N. Lombard, J. J. Riley, and E. A. D'Asaro, 1995: Available potential energy and mixing in density-stratified fluids. *Journal of Fluid Mechanics*, **289**, 115–128, <https://doi.org/doi.org/10.1017/S002211209500125X>.

Wong, K., R. Tailleux, and S. L. Gray, 2016: The computation of reference state and ape production by diabatic processes in an idealized tropical cyclone. *Quarterly Journal of the Royal Meteorological Society*, **142** (700), 2646–2657, <https://doi.org/doi.org/10.1002/qj.2854>.

Wyrtki, K., 1975: El niño—the dynamic response of the equatorial pacific ocean to atmospheric forcing. *Journal of Physical Oceanography*, **5** (4), 572–584, [https://doi.org/doi.org/10.1175/1520-0485\(1975\)005\(0572:ENTDRO\)2.0.CO;2](https://doi.org/doi.org/10.1175/1520-0485(1975)005(0572:ENTDRO)2.0.CO;2).

Wyrtki, K., 1981: An estimate of equatorial upwelling in the pacific. *Journal of Physical Oceanography*, **11** (9), 1205–1214, [https://doi.org/doi.org/10.1175/1520-0485\(1981\)011\(1205:AEOEUI\)2.0.CO;2](https://doi.org/doi.org/10.1175/1520-0485(1981)011(1205:AEOEUI)2.0.CO;2).

Xie, S.-P., C. Deser, G. A. Vecchi, J. Ma, H. Teng, and A. T. Wittenberg, 2010: Global warming pattern formation: Sea surface temperature and rainfall. *Journal of Climate*, **23** (4), 966–986, <https://doi.org/doi.org/10.1175/2009JCLI3329.1>.

Zebiak, S. E., and M. A. Cane, 1987: A model el niño–southern oscillation. *Monthly Weather Review*, **115** (10), 2262–2278, [https://doi.org/doi.org/10.1175/1520-0493\(1987\)115\(2262:AMENO\)2.0.CO;2](https://doi.org/doi.org/10.1175/1520-0493(1987)115(2262:AMENO)2.0.CO;2).

Zemskova, V. E., B. L. White, and A. Scotti, 2015: Available potential energy and the general circulation: Partitioning wind, buoyancy forcing, and diapycnal mixing. *Journal of Physical Oceanography*, **45** (6), 1510–1531, <https://doi.org/doi.org/10.1175/JPO-D-14-0043.1>.

Zhuo, J.-Y., C.-Y. Lee, A. Sobel, R. Seager, S. J. Camargo, Y.-H. Lin, B. Fosu, and K. A. Reed, 2024: A more la niña-like response to radiative forcing after flux adjustment in cesm2. *Journal of Climate*, <https://doi.org/doi.org/10.1175/JCLI-D-24-0331.1>.